Journal of Medicinal Chemistry

Article

pubs.acs.org/jmc

Development of ^{18}F-Labeled Picolinamide Probes for PET Imaging of Malignant Melanoma

Hongguang Liu,[†] Shuanglong Liu,[†] Zheng Miao,[†] Zixin Deng,[‡] Baozhong Shen,[§] Xuechuan Hong,[‡] and Zhen Cheng*,[†]

[†]Molecular Imaging Program at Stanford (MIPS), Bio-X Program, Department of Radiology, Stanford University, California, 94305-5344, United States

[‡]Key Laboratory of Combinatorial Biosynthesis and Drug Discovery, Wuhan University, Ministry of Education, Wuhan University School of Pharmaceutical Sciences, Wuhan 430071, People's Republic of China

[§]Department of Radiology, Fourth Affiliated Hospital of Harbin Medical University, Harbin 150001, People's Republic of China

Supporting Information

ABSTRACT: Melanoma is an aggressive skin cancer with worldwide increasing incidence. Development of positron emission tomography (PET) probes for early detection of melanoma is critical for improving the survival rate of melanoma patients. In this research, ^{18}F-picolinamide-based PET probes were prepared by direct radiofluorination of the bromopicolinamide precursors using no-carrier-added ^{18}F-fluoride. The resulting probes, ^{18}F-**1**, ^{18}F-**2** and ^{18}F-**3**, were then evaluated *in vivo* by small animal PET imaging and biodistribution studies in C57BL/6 mice bearing B16F10 murine melanoma tumors. Noninvasive small animal PET studies demonstrated excellent tumor imaging contrasts for all probes, while ^{18}F-**2** showed higher tumor to muscle ratios than ^{18}F-**1** and ^{18}F-**3**. Furthermore, ^{18}F-**2** demonstrated good *in vivo* stability as evidenced by the low bone uptake in biodistribution studies. Collectively, these findings suggest ^{18}F-**2** as a highly promising PET probe for translation into clinical detection of melanoma.

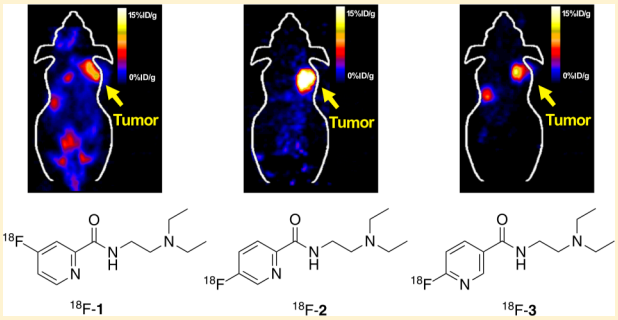

INTRODUCTION

Malignant melanoma is one of the most aggressive and lethal cancers and has increasing incidence world wide, especially in the Caucasian population.[1,2] Its strong tendency to metastasize and the absence of effective treatment for advanced diseases result in a poor overall survival.[3,4] Therefore, development of novel and accurate molecular imaging techniques to detect melanoma at its earliest stages is critical for improving the survival of patients that have malignant melanoma.

Over the last a few decades, noninvasive molecular imaging of malignant melanoma with various modalities has been extensively studied; these modalities include radionuclide imaging with positron emission tomography (PET) and single photon emission computed tomography (SPECT), magnetic resonance imaging (MRI), computed tomography (CT), and ultrasound (US) imaging. The higher sensitivity of PET and SPECT than the traditional imaging methods such as MRI, CT, and US has attracted more and more research interest on developing nuclear imaging agents for melanoma detection.[5] Especially, PET imaging with ^{18}F-fluoro-deoxyglucose (^{18}F-FDG) has demonstrated much higher sensitivity and specificity than that obtained by CT, ultrasound, radiography, and liver function tests and histology or clinical follow-up.[6] Furthermore, ^{18}F-FDG PET was shown to detect malignant melanoma up to 6 months earlier than those conventional techniques.[7,8] However, because the uptake and cellular retention of ^{18}F-FDG involve increased glucose metabolism, which also occurs in many other tumor types or in surgical wounds, pneumonia, and infection/inflammation conditions, ^{18}F-FDG lacks high specificity for melanoma imaging, and false-positive detections often happen.[6,7,9]

Nuclear imaging modalities (SPECT and PET) heavily rely on probes for monitoring specific molecular targets or pathways *in vivo*. Nuclear probes with high specificity based on different targeting or molecular recognition mechanisms help to increase the effectiveness of PET or SPECT for melanoma detection. Therefore, many radiolabeled probes for imaging different molecular targets or processes associated with malignant melanoma have been designed and evaluated for melanoma imaging, such as monoclonal antibodies against melanoma-associated antigens,[10,11] iodoamphetamine,[12] α-melanocyte-stimulating hormone peptides,[13−17] or benzamide (BZA)-based compounds.[18−20] So far, BZA analogs have been shown to be among the most promising melanoma targeting agents for both diagnosis and therapeutic applications. An *in vitro* cell study

Received: September 19, 2012
Published: January 9, 2013

demonstrated the high binding affinity of BZA analogs to melanin that is present in melanoma.[21] Moreover, a clinical study using ^{123}I-labeled BZA for detecting malignant melanoma and its metastases revealed 81% diagnostic sensitivity, 87% accuracy, and 100% specificity.[22] Consequently, ^{18}F-labeled BZA (^{18}F-FBZA, Figure 1D) has been developed for PET imaging of

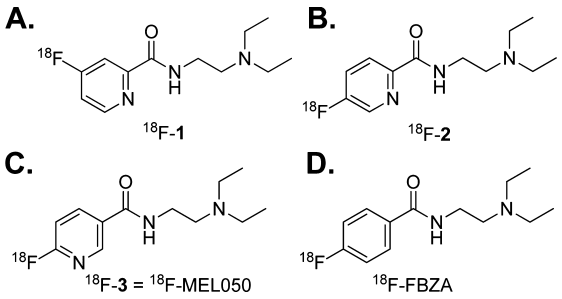

Figure 1. The chemical structures of ^{18}F-**1**, ^{18}F-**2**, ^{18}F-**3** (^{18}F-MEL050), and ^{18}F-FBZA.

melanoma and its metastases using mice bearing B16F10 melanoma tumors.[23,24] It was reported that the B16F10 tumor uptake at 2 h postinjection (p.i.) reached 5.94 ± 1.83 percentage injected dose per gram (%ID/g).[23] However, the multistep radiosynthesis of ^{18}F-FBZA could be a bottleneck for its large production and potential clinical translation.

Recently the pyridine-based precursor ^{18}F-6-fluoro-*N*-[2-(diethylamino)ethyl] pyridine-3-carboxamide (^{18}F-MEL050, Figure 1C) was successfully synthesized in single step with high radiochemical yield (RCY). This novel PET probe displays excellent performance for imaging of primary and metastatic melanoma.[25−27] In pigmented melanoma B16-F0 xenografts, ^{18}F-MEL050 exhibits high tumor uptake and tumor-to-background ratio of approximately 50:1 at 2 h p.i. of the probe. The excellent *in vivo* performance of ^{18}F-MEL050, plus its easy radiosynthesis, encouraged us to design and biologically evaluate more ^{18}F-MEL050 analogs for melanoma imaging. More specifically, *N*-(2-(diethylamino)ethyl)-^{18}F-4-fluoropicolinamide (shortened as ^{18}F-**1**, Figure 1A) and *N*-(2-(diethylamino)-ethyl)-^{18}F-5-fluoropicolinamide (shortened as ^{18}F-**2**, Figure 1B) were synthesized and compared side-by-side with ^{18}F-MEL050 (shorted as ^{18}F-**3**, Figure 1C) by small animal PET imaging and biodistribution studies in B16F10-tumor bearing mice.

RESULTS

Chemistry and Radiochemistry. The authentic ^{19}F-fluorine compounds (^{19}F-**1**, ^{19}F-**2**, and ^{19}F-**3**), and their precursors (**4**, **5**, and **6**, Scheme 1) for ^{18}F-fluorination were prepared by condensation of a bromopicolinic acid or bromoniconitic acid with *N*,*N*-diethylethylenediamine (DEED) via *O*-(*N*-succinimidyl)-1,1,3,3-tetramethyl-uronium tetrafluoroborate (TSTU) activation in the presence of diisopropylethylamine (DIPEA) (Scheme 1 and Supporting Information). The azeotropically dried ^{18}F-fluoride can replace the bromo leaving group in each precursor to make the corresponding product in one step. Hence, all of the ^{18}F-labeled products were prepared within 1 h, including reversed-phase high-performance liquid chromatography (RP-HPLC) purification and product formulation for further biological evaluation. The resultant products, ^{18}F-**1**, ^{18}F-**2**, and ^{18}F-**3**, were prepared in radiochemical yields of 24.5% ± 6.7%, 9.5% ± 1.9%, and 21.5% ± 15.5% (n = 3, non-decay-corrected), respectively. All of the ^{18}F probes were

Scheme 1. Synthetic Schemes for Preparation of the Precursors for ^{18}F-Fluorination and ^{19}F Authentic Standards

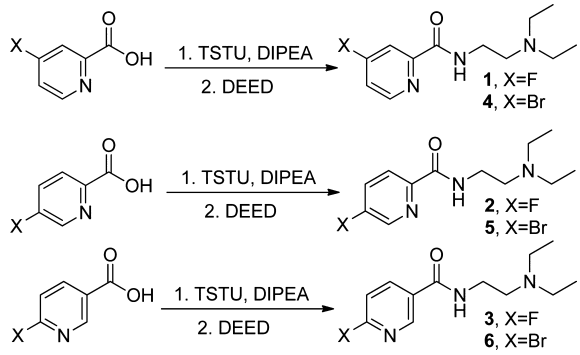

produced in more than 95% radiochemical purity and free of the corresponding bromo-precursors, as demonstrated by quality control analysis (RP-HPLC). The specific activity for these PET probes was in the range of 100−150 GBq/μmol.

Small Animal PET Imaging Studies. The tumor-targeting efficacy and imaging properties of ^{18}F-**1** and ^{18}F-**2** were evaluated in B16F10 tumor-bearing mice, and the results were compared with ^{18}F-**3**, which was examined in the same tumor model. In static small animal PET scans, representative coronal images of B16F10 tumor bearing mice (n = 4) at different times after intravenous injection of about 3.7 MBq (100 μCi) of ^{18}F-**1**, ^{18}F-**2**, or ^{18}F-**3** are shown in Figure 2. B16F10 tumors were clearly

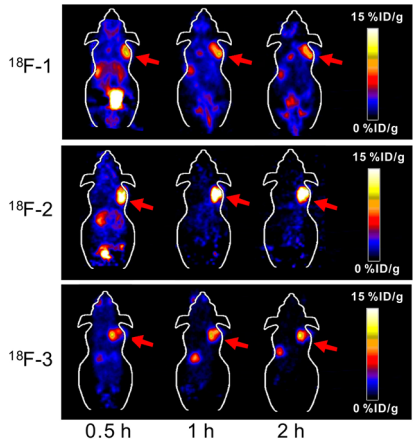

Figure 2. Decay-corrected whole-body coronal small animal PET images of C57BL/6 mice bearing B16F10 murine melanomas from a static scan at 0.5, 1, and 2 h after injection of ^{18}F-**1**, ^{18}F-**2**, and ^{18}F-**3**. Tumors are indicated by arrows.

visualized with high tumor-to-background contrast at all time points from 0.5 to 2 h. The highest uptakes observed in the kidneys at early time points suggested that these PET probes were mainly excreted through the renal system. Quantification analysis of tumors and other major organ activity accumulation in PET images was done by analyzing the regions of interest (ROI) that circle the entire organ on the coronal images. The tumor uptakes of ^{18}F-**1** were determined to be 9.52 ± 1.27, 8.97 ± 1.76, and 9.73 ± 1.41 %ID/g at 0.5, 1, and 2 h. The tumor uptakes of ^{18}F-**3** were determined to be 7.54 ± 1.60, 7.94 ± 0.96, and 8.47 ± 1.35 %ID/g at 0.5, 1, and 2 h. ^{18}F-**1** and ^{18}F-**3** had much lower tumor uptake compared with ^{18}F-**2**, which were 12.74 ± 1.70, 16.61 ± 2.60, and 16.87 ± 1.23 %ID/g at 0.5, 1, and 2 h, respectively (Figure 3A−C).

dx.doi.org/10.1021/jm301740k | J. Med. Chem. 2013, 56, 895−901

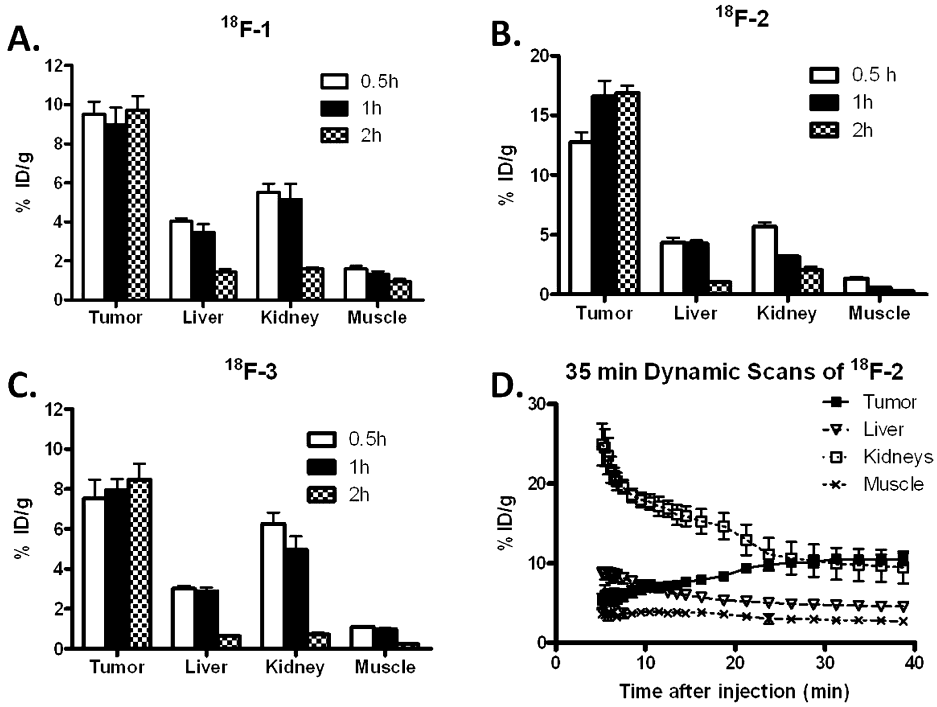

Figure 3. Small animal PET images quantification of tumors and major organs at 0.5 h, 1 h, and 2 h after injection of (A) ^{18}F-**1**, (B) ^{18}F-**2**, and (C) ^{18}F-**3** (~100 μCi/mouse, n = 4). (D) Time–activity curves of tumor and major organs of C57BL/6 mice bearing B16F10 murine melanoma tumors from 35 min dynamic scans after intravenous injection of ^{18}F-**2** (~100 μCi/mouse, n = 4).

Table 1. Biodistributions of ^{18}F-1, ^{18}F-2, and ^{18}F-3 in C57BL/6 Mice Bearing B16F10 Murine Melanoma Tumors at 1 and 2 h p.i.[a]

	^{18}F-1		^{18}F-2		^{18}F-3	
organ	1 h	2 h	1 h	2 h	1 h	2 h
tumor	7.54 ± 1.64[b]	8.66 ± 1.42[b]	15.20 ± 3.37[b,c]	16.97 ± 3.28[b,c]	9.54 ± 3.44[c]	9.29 ± 2.49[c]
blood	0.33 ± 0.08	0.15 ± 0.01[b]	0.42 ± 0.13	0.19 ± 0.02[b]	0.46 ± 0.07	0.20 ± 0.01
heart	0.60 ± 0.07[b]	0.37 ± 0.04[b]	1.17 ± 0.26[b]	0.59 ± 0.04[b,c]	1.54 ± 0.53	0.40 ± 0.06[c]
lungs	0.88 ± 0.13[b]	0.59 ± 0.08	1.58 ± 0.33[b]	0.69 ± 0.07[c]	1.52 ± 0.43	0.92 ± 0.13[c]
liver	2.07 ± 0.47[b]	1.41 ± 0.12[b]	4.71 ± 1.47[b]	3.32 ± 0.39[b,c]	4.47 ± 2.27	1.07 ± 0.25[c]
spleen	1.09 ± 0.87	0.31 ± 0.02	1.78 ± 0.49	1.13 ± 0.87	2.88 ± 1.63	0.56 ± 0.06
pancreas	1.06 ± 0.36	0.44 ± 0.02[b]	1.61 ± 0.48	0.61 ± 0.04[b]	3.58 ± 1.69	0.71 ± 0.07
stomach	2.24 ± 0.60	1.64 ± 0.59	4.26 ± 2.62	1.47 ± 0.53	5.03 ± 1.78	2.27 ± 0.33
brain	0.49 ± 0.14[b]	0.24 ± 0.03[b]	1.28 ± 0.33[b]	0.42 ± 0.06[b]	1.56 ± 0.41	0.41 ± 0.07
intestine	2.28 ± 0.36	0.98 ± 0.04	2.01 ± 0.47	0.88 ± 0.21	3.46 ± 1.26	0.89 ± 0.53
kidneys	1.34 ± 0.28	0.69 ± 0.06[b]	3.32 ± 1.23	1.03 ± 0.09[b]	5.63 ± 1.72	1.20 ± 0.29
skin	0.73 ± 0.16[b]	0.63 ± 0.35	1.30 ± 0.48[b]	0.68 ± 0.41	2.37 ± 0.64	0.71 ± 0.39
muscle	0.60 ± 0.14[b]	0.20 ± 0.03	1.16 ± 0.29[b]	0.41 ± 0.04[b]	1.11 ± 0.18	0.52 ± 0.08
bone	11.29 ± 2.88[b]	10.27 ± 3.59[b]	2.40 ± 0.26[b]	1.72 ± 0.45[b]	3.48 ± 0.80	2.12 ± 0.38
eyes	35.96 ± 12.17	32.45 ± 3.67	37.47 ± 2.55	32.83 ± 5.25	34.00 ± 9.19	32.23 ± 7.73
			Uptake Ratio			
tumor to blood	28.32 ± 3.32[b]	44.33 ± 7.35[b]	41.44 ± 8.09[b,c]	88.25 ± 9.77[b,c]	20.44 ± 4.34[c]	39.20 ± 4.66[c]
tumor to lung	8.81 ± 2.44	9.46 ± 1.76[b]	9.94 ± 1.29[c]	24.92 ± 6.56[b,c]	6.23 ± 0.84[c]	10.49 ± 4.33[c]
tumor to liver	3.85 ± 1.32	4.16 ± 1.25	3.79 ± 1.41	5.14 ± 1.03	2.24 ± 0.32	7.26 ± 3.33
tumor to muscle	13.12 ± 4.15	27.75 ± 4.24[b]	13.84 ± 2.38	36.79 ± 5.21[b,c]	11.24 ± 2.76	15.22 ± 3.91[c]

[a]Data are expressed as normalized accumulation of activity in %ID/g ± SD (n = 4). [b]P < 0.05, comparison of biodistribution between ^{18}F-**1** and ^{18}F-**2**. [c]P < 0.05, comparison of biodistribution between ^{18}F-**2** and ^{18}F-**3**.

The higher tumor uptake of ^{18}F-**2** encouraged us to perform a 35-min dynamic small animal PET scans for this novel probe (n = 4). As shown in Figure 3D, ^{18}F-**2** was rapidly cleared from renal system as determined by ROI analysis of the kidneys. At 5 min after tail vein injection of ^{18}F-**2**, radioactivity rapidly accumulated in kidneys (24.91 ± 5.29 %ID/g) and decreased to 9.44 ± 4.04 % ID/g at 35 min p.i. In contrast, tumor uptake reached 5.28 ± 1.54 %ID/g at 5 min p.i. and gradually increased to the highest 10.52 ± 1.29 %ID/g at the end of the 35 min dynamic scan. During the whole dynamic scan frames, low levels of liver and muscle uptakes were observed.

Biodistribution Studies. We also performed a biodistribution experiment by direct-sampling tumors and tissues of interest. The results are shown in Table 1. The B16F10 tumor

dx.doi.org/10.1021/jm301740k | J. Med. Chem. 2013, 56, 895–901

uptakes for ^{18}F-**1** were 7.54 ± 1.64 and 8.66 ± 1.42 %ID/g at 1 and 2 h, respectively, while for ^{18}F-**3**, they were 9.54 ± 3.44 and 9.29 ± 2.49 %ID/g at 1 and 2 h p.i. Both ^{18}F-**1** and ^{18}F-**3** have lower uptake than ^{18}F-**2**, which were 15.20 ± 3.37 %ID/g and 16.97 ± 3.28 %ID/g at 1 and 2 h p.i., respectively. Of note, because of the high melanin concentration in C57BL/6 mouse eyes, the uptake in eyes remained at high levels for all three probes. Interestingly, the bone uptake of ^{18}F-**2** (2.40 ± 0.26 and 1.72 ± 0.45 %ID/g at 1 and 2 h, respectively, n = 4) and ^{18}F-**3** (3.48 ± 0.80 and 2.12 ± 0.38 %ID/g at 1 and 2 h, respectively, n = 4) were significantly lower than those of ^{18}F-**1** (11.29 ± 2.88 and 10.27 ± 3.59 %ID/g at 1 and 2 h, respectively, n = 4) ($P < 0.05$), which indicated that ^{18}F-**2** and ^{18}F-**3** have better *in vivo* stability against defluorination. In comparison, ^{18}F-**1** showed significant defluorination *in vivo* as demonstrated by its high bone uptake. Moreover, because of the rapid clearance of these ^{18}F-labeled picolinamide probes from normal nontargeted organs, most of the tumor-to-normal tissue ratios increase with time. For example, the tumor to muscle ratio of ^{18}F-**2** was 13.84 ± 2.38 and 36.79 ± 5.21 at 1 and 2 h, respectively; while for ^{18}F-**3**, it was 11.24 ± 2.76 and 15.22 ± 3.91 at 1 and 2 h p.i., respectively (Table 1).

DISCUSSION AND CONCLUSIONS

^{18}F ($t_{1/2}$ = 109.7 min; β^+, 99%) is an ideal PET radionuclide for labeling biologically active ligands such as small molecules, peptides, or small proteins for PET probe development. The success of ^{18}F-FDG has made PET a powerful tool in cancer diagnosis, patient stratification, and treatment monitoring of cancer patients.[28] In the development of melanoma-specific imaging probes other than the generic tumor imaging probes such as ^{18}F-FDG, ^{123}I-labeled BZA compounds have been evaluated in melanoma patients with 100% specificity.[22] Because of favorable physical properties of ^{18}F-fluoride, efforts have been made to develop ^{18}F-labeled BZA (^{18}F-FBZA)[23,24] and ^{18}F-labeled BZA-like ^{18}F-MEL050 (^{18}F-**3**).[27] It has been found that ^{18}F-**3** offers high tumor uptakes, fast clearance, and low background.[27] The syntheses of ^{18}F-**3** analogs have been optimized recently; however, *in vivo* tumor targeting efficacy was not reported therein.[29] To further develop ^{18}F-**3** analogs with improved *in vivo* performance, we designed and synthesized ^{18}F-**1** and ^{18}F-**2** herein and compared their *in vivo* tumor imaging properties with ^{18}F-**3** in the same B16F10 melanoma model.

The authentic standards (**1**−**3**) and nonradioactive precursors (**4**−**6**) can be readily prepared in high yields from their corresponding acids. The compounds **1**−**6** were fully characterized using nuclear magnetic resonance (NMR) and electrospray ionization mass spectrometry (ESI-MS). The direct and single step ^{18}F-fluorination of the precursors can be easily accomplished to achieve the targeted PET probes in good radiochemical yields. Because of the low reactivity of the 3-position, the RCYs of ^{18}F-**2** are lower than the other two radioligands ($P < 0.05$). However, the radiosynthesis of ^{18}F-**2** can still be easily automated for large quantity synthesis (3.7−37 GBq) for potential clinical translation, because of the short synthetic time and the straightforward radiochemistry.

As expected, ^{18}F-**1**, ^{18}F-**2**, and ^{18}F-**3** all exhibit high tumor targeting efficiency, excellent tumor imaging contrasts, and desirable biodistribution patterns (Figure 2, Table 1). Particularly, ^{18}F-**2** shows significantly lower bone uptake than ^{18}F-**1** and ^{18}F-**3** ($P < 0.05$) (Table 1). Because of the high reactivity of 2- and 4-positions of the pyridine ring toward the nucleophilic aromatic substitution,[30] some weak nucleophiles, such as water, amino acid, or proteins, can potentially replace the ^{18}F in these two positions. In contrast, the relative low reactivity of 3-position in the pyridine ring increases the relative *in vivo* stability of ^{18}F-**2**. It is noteworthy that the bone uptake of ^{18}F-**1** is about 10 times higher than that of ^{18}F-**2** or ^{18}F-**3**, which suggests ^{18}F in the 4-position is very unstable (Table 1).

In our previous study, ^{18}F-FBZA was developed as a melanin-targeting PET probe with a chemical structure similar to that of ^{18}F-**2**.[23] However, ^{18}F-FBZA has a much lower tumor uptake in the B16F10 melanoma tumors than ^{18}F-**2** (5.94 ± 1.83 %ID/g for ^{18}F-FBZA at 2 h p.i. vs. 16.97 ± 3.28 %ID/g for ^{18}F-**2** at 2 h p.i.). Furthermore, a three-step radiosynthesis of *N*-succinimidyl 4-^{18}F fluorobenzoate (^{18}F-SFB) is needed before direct coupling of the ^{18}F-SFB with the amine compound to prepare ^{18}F-FBZA; thus the total radiosynthesis time is typically more than 3 h, compared with only 1 h for preparation ^{18}F-**1** and ^{18}F-**2**. In this study, we also show that ^{18}F-**2** is superior to ^{18}F-**3** in terms of tumor uptake, tumor to normal organ ratios (Table 1), and tumor imaging contrast (Figure 2). Overall, ^{18}F-**2** is demonstrated to be an excellent candidate for translation as a clinical PET probe for melanoma diagnosis in term of radiosynthesis, tumor targeting efficiency, and *in vivo* stability.

In conclusion, we designed and synthesized two novel PET probes and a reported PET probe for melanoma diagnosis based on the picolinamide structure. The small animal PET and biodistribution studies in murine melanoma xenografts resulted in excellent tumor imaging contrast using all of these probes. Especially ^{18}F-**2** shows high *in vivo* stability and favorable pharmacokinetic properties such as fast clearance from urinal system and almost background level of uptake for all of the major organs at 2 h. The high selectivity and specificity of ^{18}F-**2**, as evidenced by the high tumor-to-non tumor ratios, highlight that ^{18}F-**2** PET has high potential to improve melanoma detection. All the desirable properties of ^{18}F-**2** warrant large scale production and potential clinical applications of this novel PET probe.

EXPERIMENTAL SECTION

General. All chemicals obtained commercially were of analytic grade and used without further purification. No-carrier-added ^{18}F-fluoride was obtained from an in-house PETtrace cyclotron (GE Healthcare). Reversed-phase extraction C18 Sep-Pak cartridges were obtained from Waters and were pretreated with ethanol and water before use. The syringe filter and polyethersulfone membranes (pore size, 0.22 μm; diameter, 13 mm) were obtained from Nalge Nunc International. The semipreparative RP-HPLC using a Vydac protein and peptide column (218TP510; 5 μm, 250 mm × 10 mm) was performed on a Dionex 680 chromatography system with a UVD 170U absorbance detector and model 105S single-channel radiation detector (Carroll & Ramsey Associates). The recorded data were processed using Chromeleon version 6.50 software. With a flow rate of 5 mL/min, the mobile phase was changed from 95% solvent A [0.1% trifluoroacetic acid (TFA) in water] and 5% B [0.1% TFA in acetonitrile (MeCN)] (0−2 min) to 35% solvent A and 65% solvent B at 32 min. Analytical RP-HPLC has the same gradient system except that the flow rate was 1 mL/min with a Vydac protein and peptide column (218TP510; 5 μm, 250 mm × 4.6 mm). The UV absorbance was monitored at 218 nm, and the identification of the small molecules was confirmed based on the UV spectrum acquired using a PDA detector. All synthesized compounds showed more than 95% purity (RP-HPLC). Small animal PET scans were performed on a microPET R4 rodent model scanner (Concorde Microsystems Inc.). The scanner has a computer-controlled bed and 10.8 cm transaxial and 8 cm axial fields of view (FOVs). It has no septa and operates exclusively in the three-dimensional (3D) list mode.

Animals were placed near the center of the FOV of the scanner, where the highest image resolution and sensitivity are available.

Chemistry and Radiochemistry. Preparation of ^{19}F-**1**, ^{19}F-**2**, and ^{19}F-**3** and their bromo-precursors **4**, **5**, and **6** (Scheme 1 and Supporting Information) was accomplished using the same protocol. As an example, ^{19}F-**1** was synthesized as follows: To a solution of 4-fluoropicolinic acid (5.0 mg, 35.5 μmol) in 200 μL of *N*,*N*-dimethylformamide (DMF) was added TSTU (10.0 mg, 33.0 μmol) and 20 μL of DIPEA. After incubating at 60 °C for 3 h, the reaction mixture was cooled to room temperature, followed by addition of *N*,*N*-diethylethylenediamine (7.0 mg, 60 μmol). After 2 h, the mixture was diluted with 1 mL of 5% acetic acid solution. The product ^{19}F-**1** was isolated by semipreparative RP-HPLC. The collected fractions were combined, and acetonitrile was removed under reduced pressure. The final product was obtained by lyophilization.

*N-(2-(Diethylamino)ethyl)-4-fluoropicolinamide (^{19}F-**1**).* The product was obtained as white powder in the yield of 56% with 98% purity as determined by RP-HPLC. ESI-MS: *m*/*z* 240.3 $[M + H]^+$ ($C_{12}H_{19}FN_3O$, calculated molecular weight 240.2). ^{1}H NMR ($CDCl_3$, 300 MHz): δ = 8.94 (br, 1H), 8.57 (dd, *J* = 5.2 Hz, 9.0 Hz, 1H), 7.83 (dd, *J* = 2.4 Hz, 9.0 Hz, 1H), 7.15 (dd, *J* = 2.4 Hz, 5.2 Hz, 1H), 3.93 (t, *J* = 6.1 Hz, 2H), 3.29 (t, *J* = 5.9 Hz, 2H), 3.22 (q, *J* = 8.6 Hz, 4H), 1.37 (t, *J* = 7.1 Hz, 6H). ^{13}C NMR ($CDCl_3$, 75 MHz): δ = 167.9, 164.6 (d, $J_{C,F}$ = 101.8 Hz), 152.5, 151.2 (d, $J_{C,F}$ = 6.6 Hz), 114.2 (d, $J_{C,F}$ = 16.5 Hz), 110.4 (d, $J_{C,F}$ = 18.7 Hz), 51.2, 47.3, 35.0, 8.4.

*N-(2-(Diethylamino)ethyl)-5-fluoropicolinamide (^{19}F-**2**).* The product was obtained as white powder in the yield of 75% with 98% purity as determined by RP-HPLC. ESI-MS: *m*/*z* 240.5 $[M + H]^+$ ($C_{12}H_{19}FN_3O$, calculated molecular weight 240.2). ^{1}H NMR ($CDCl_3$, 300 MHz): δ = 11.35 (br, 1H), 8.41 (d, *J* = 2.7 Hz, 1H), 8.17 (dd, *J* = 4.4, 8.2 Hz, 1H), 7.45 (dd, *J* = 2.7, 8.2 Hz, 1H), 3.88 (t, *J* = 6.1 Hz, 2H), 3.38−3.08 (m, 6H), 1.36 (t, *J* = 7.3 Hz, 6H). ^{13}C NMR ($CDCl_3$, 75 MHz): δ = 164.9, 161.5 (d, $J_{C,F}$ = 38.5 Hz), 161.4 (d, $J_{C,F}$ = 261.5 Hz), 145.2 (d, $J_{C,F}$ = 4.5 Hz), 137.3 (d, $J_{C,F}$ = 25.4 Hz), 124.0 (d, $J_{C,F}$ = 5.4 Hz), 51.5, 47.2, 34.8, 8.3.

*N-(2-(Diethylamino)ethyl)-6-fluoronicotinamide (^{19}F-**3**).* The product was obtained as white powder in the yield of 62% with 97% purity as determined by RP-HPLC. ESI-MS: *m*/*z* 240.3 $[M + H]^+$ ($C_{12}H_{19}FN_3O$, calculated molecular weight 240.2). ^{1}H NMR ($CDCl_3$, 300 MHz): δ = 11.00 (br, 1H), 8.80 (d, *J* = 1.7 Hz, 1H), 8.33 (dd, *J* = 1.7, 8.5 Hz, 1H), 6.99 (dd, *J* = 1.7, 8.5 Hz, 1H), 3.82 (t, *J* = 3.9 Hz, 2H), 3.37 (t, *J* = 3.9 Hz, 2H), 3.23 (q, *J* = 7.3 Hz, 2H), 1.35 (t, *J* = 7.3 Hz, 6H). ^{13}C NMR ($CDCl_3$, 75 MHz): δ = 167.0, 164.6 (d, $J_{C,F}$ = 137.4 Hz), 148.7 (d, $J_{C,F}$ = 15.9 Hz), 140.4 (d, $J_{C,F}$ = 9.3 Hz), 127.1 (d, $J_{C,F}$ = 4.4 Hz), 109.5 (d, $J_{C,F}$ = 37.4 Hz), 52.4, 48.6, 35.8, 8.6.

*4-Bromo-N-(2-(diethylamino)ethyl)picolinamide (**4**).* The product was obtained as white powder in the yield of 82% with 97% purity as determined by RP-HPLC. ESI-MS: *m*/*z* 300.4 $[M + H]^+$ ($C_{12}H_{19}BrN_3O$, calculated molecular weight 300.1). ^{1}H NMR ($CDCl_3$, 300 MHz): δ = 8.97 (br, 1H), 8.40 (d, *J* = 5.2 Hz, 1H), 8.28 (d, *J* = 1.7 Hz, 1H), 7.61 (dd, *J* = 1.7, 3.2 Hz, 1H), 3.91 (t, *J* = 3.7 Hz, 2H), 3.39 (t, *J* = 3.7 Hz, 2H), 3.23 (q, *J* = 7.1 Hz, 4H), 1.34 (t, *J* = 7.1 Hz, 6H). ^{13}C NMR ($CDCl_3$, 75 MHz): δ = 164.5, 150.2, 149.5, 134.3, 129.8, 125.8, 51.2, 47.1, 34.9, 8.3.

*5-Bromo-N-(2-(diethylamino)ethyl)picolinamide (**5**).* The product was obtained as white powder in the yield of 90% with 98% purity as determined by RP-HPLC. ESI-MS: *m*/*z* 300.4 $[M]^+$ ($C_{12}H_{19}BrN_3O$, calculated molecular weight 300.1). ^{1}H NMR ($CDCl_3$, 300 MHz): δ = 8.90 (br, 1H), 8.62 (s, 1H), 8.01−7.95 (m, 1H), 7.61 (dd, *J* = 1.7, 3.2 Hz, 1H), 3.89 (t, *J* = 5.8 Hz, 2H), 3.26 (t, *J* = 5.8 Hz, 2H), 3.25 (q, *J* = 7.3 Hz, 4H), 1.34 (t, *J* = 7.3 Hz, 6H). ^{13}C NMR ($CDCl_3$, 75 MHz): δ = 165.1, 149.9, 147.4, 140.0, 124.6, 123.5, 51.4, 47.3, 34.8, 8.3.

*6-Bromo-N-(2-(diethylamino)ethyl)nicotinamide (**6**).* The product was obtained as white powder in the yield of 78% with 97% purity as determined by RP-HPLC. ESI-MS: *m*/*z* 300.2 $[M + H]^+$ ($C_{12}H_{19}BrN_3O$, calculated molecular weight 300.1). ^{1}H NMR ($CDCl_3$, 300 MHz): δ = 9.38 (br, 1H), 8.92 (s, 1H), 8.08 (d, *J* = 8.3 Hz, 1H), 7.55 (d, *J* = 8.3 Hz, 1H), 3.84 (m, 2H), 3.34 (m, 2H), 3.21 (m, 4H), 1.35 (t, *J* = 7.1 Hz, 6H). ^{13}C NMR ($CDCl_3$, 75 MHz): δ = 165.8, 150.1, 145.7, 137.2, 128.0, 123.8, 52.3, 48.6, 35.7, 8.

Radiochemistry. An aqueous ^{18}F-fluoride solution (15−30 mCi) was added to a 10 mL vial containing anhydrous acetonitrile (1 mL), $K_{2.2.2}$ (15 mg), and K_2CO_3 (3 mg). The solvent was evaporated under a stream of argon at 100 °C under vacuum to produce the $K^{18}F$−$K_{2.2.2}$ complex. This azeotropic drying was repeated twice by anhydrous acetonitrile (2 × 1 mL). The bromo-precursor (**4**, **5**, or **6**, 5 mg) was dissolved in anhydrous DMSO (200 μL) and added to the dried $K^{18}F$−$K_{2.2.2}$ complex. The reaction was stirred and heated at 110 °C for 10 min and cooled to room temperature. The mixture was then diluted with 1 mL of 5% acetic acid solution for RP-HPLC purification. The collected radioactive peak was dried using a rotary evaporator and the radiolabeled products were reconstituted in phosphate-buffered saline (PBS, 0.1 M, pH = 7.4) and passed through a 0.22 μm Millipore filter into a sterile vial for *in vitro* and *in vivo* experiments. The radiochemical yields were calculated based on the obtained radioactive product divided by the activity loaded into the reaction vessel.

Cell Culture. B16F10 cells were cultured in Dulbecco's modified Eagle high-glucose medium (Gibco Life Sciences) supplemented with 10% fetal bovine serum with penicillin and streptomycin. The cells were regularly maintained in a 37 °C, 5% CO_2 humidified incubator.

Animal Biodistribution Studies. Animal procedures were performed according to a protocol approved by the Stanford University Institutional Animal Care and Use Committee. All of the animals were purchased from Charles River Laboratory. Cultured B16F10 cells (∼1.0 × 10^6) were suspended in PBS and subcutaneously implanted in the right shoulder of C57BL/6 mice. Tumors were allowed to grow to a size of 0.5 cm (∼10 day) before use. For biodistribution studies, the tumor-bearing mice (*n* = 4 for each group) were injected with about 3.7 MBq (100 μCi) of ^{18}F-**1**, ^{18}F-**2**, or ^{18}F-**3** through the tail vein and sacrificed at 1.0 and 2.0 h p.i. Tumor and normal tissues of interest were removed and weighed, and their radioactivity was measured in a γ-counter. The radioactivity uptake in the tumor and normal tissues was calculated as % ID/g.

Small Animal PET Imaging. For dynamic scan, B16F10 tumor-bearing mice (*n* = 4) were injected via the tail vein with approximately 3.7 MBq (100 μCi) of ^{18}F-**2**, and scans (6 × 20 s, 8 × 60 s, 10 × 150 s, total of 24 frames) were started roughly 2.0 min after the injection of the probe and continued for 35 min. For static scans, the mice bearing B16F10 (*n* = 4 for each probe) tumor xenografts were injected with about 3.7 MBq (100 μCi) of ^{18}F-**1**, ^{18}F-**2**, or ^{18}F-**3** via the tail vein. At 0.5, 1, and 2 h p.i., the mice were anesthetized with isoflurane (5% for induction and 2% for maintenance in 100% O_2) using a knock-down box. With the help of a laser beam attached to the scanner, the mice were placed in the prone position and near the center of the field of view of the scanner. The 3-min static scans were then obtained. Images were reconstructed using two-dimensional ordered subsets expectation maximization (OSEM) algorithm. No background correction was performed. ROI (5 pixels for coronal and transaxial slices) were drawn over the tumor on decay-corrected whole-body coronal images. The maximum counts per pixel per minute were obtained from the ROI and converted to counts per milliliter per minute using a calibration constant. On the basis of the assumption of a tissue density of 1 g/mL, the ROIs were converted to counts per gram per min. Image ROI-derived %ID/g values were determined by dividing counts per gram per minute by injected dose. No attenuation correction was performed.

Statistical Analysis. Quantitative data are expressed as mean ± SD. Means were compared using the Student *t* test. *P* values of <0.05 were considered statistically significant.

■ ASSOCIATED CONTENT

Ⓢ Supporting Information

RP-HPLC and mass spectrometry data of synthesized compounds. This material is available free of charge via the Internet at http://pubs.acs.org.

AUTHOR INFORMATION

Corresponding Author

*Mailing address: Molecular Imaging Program at Stanford, Canary Center at Stanford for Cancer Early Detection Department of Radiology and Bio-X Program, 1201 Welch Road, Lucas Expansion, P095 Stanford University, Stanford, CA 94305. Phone: 650-723-7866. Fax: 650-736-7925. E-mail: zcheng@stanford.edu.

Author Contributions

H. Liu and S. Liu contributed equally. The manuscript was written through contributions of all authors. All authors have given approval to the final version of the manuscript.

Notes

The authors declare no competing financial interest.

ACKNOWLEDGMENTS

This work was supported, in part, by the Melanoma Research Alliance, National Cancer Institute (NCI) In Vivo Cellular Molecular Imaging Center (ICMIC) Grant P50 CA114747, and the international cooperation projects of the Chinese Ministry of Science and Technology (Grant 2009DFB30040). The authors thank the Radiochemistry Facility of Molecular Imaging Program at Stanford for ^{18}F-fluoride production.

ABBREVIATIONS USED

PET, positron emission tomography; BZA, benzamide; %ID/g, percentage injected dose per gram; ^{18}F-**1**, *N*-(2-(diethylamino)-ethyl)-^{18}F-4-fluoropicolinamide; ^{18}F-**2**, *N*-(2-(diethylamino)-ethyl)-^{18}F-5-fluoropicolinamide; ^{18}F-**3**(^{18}F-MEL050), ^{18}F-6-fluoro-N-[2-(diethylamino)ethyl] pyridine-3-carboxamide; RCYs, radiochemical yields

REFERENCES

(1) Jemal, A.; Siegel, R.; Ward, E.; Murray, T.; Xu, J.; Thun, M. J. Cancer statistics, 2007. *CA—Cancer J Clin.* **2007**, *57*, 43—66.

(2) Jemal, A.; Siegel, R.; Xu, J.; Ward, E. Cancer statistics, 2010. *CA—Cancer J Clin.* **2010**, *60*, 277—300.

(3) Belhocine, T. Z.; Scott, A. M.; Even-Sapir, E.; Urbain, J. L.; Essner, R. Role of nuclear medicine in the management of cutaneous malignant melanoma. *J. Nucl. Med.* **2006**, *47*, 957—967.

(4) Prichard, R. S.; Hill, A. D.; Skehan, S. J.; O'Higgins, N. J. Positron emission tomography for staging and management of malignant melanoma. *Br. J. Surg.* **2002**, *89*, 389—396.

(5) Massoud, T. F.; Gambhir, S. S. Molecular imaging in living subjects: Seeing fundamental biological processes in a new light. *Genes Dev.* **2003**, *17*, 545—580.

(6) Eigtved, A.; Andersson, A. P.; Dahlstrom, K.; Rabol, A.; Jensen, M.; Holm, S.; Sorensen, S. S.; Drzewiecki, K. T.; Hojgaard, L.; Friberg, L. Use of fluorine-18 fluorodeoxyglucose positron emission tomography in the detection of silent metastases from malignant melanoma. *Eur. J. Nucl. Med.* **2000**, *27*, 70—75.

(7) Holder, W. D., Jr.; White, R. L., Jr.; Zuger, J. H.; Easton, E. J., Jr.; Greene, F. L. Effectiveness of positron emission tomography for the detection of melanoma metastases. *Ann Surg.* **1998**, *227*, 764—769,discussion 769—771.

(8) Schwimmer, J.; Essner, R.; Patel, A.; Jahan, S. A.; Shepherd, J. E.; Park, K.; Phelps, M. E.; Czernin, J.; Gambhir, S. S. A review of the literature for whole-body FDG PET in the management of patients with melanoma. *Q. J. Nucl. Med.* **2000**, *44*, 153—167.

(9) Tyler, D. S.; Onaitis, M.; Kherani, A.; Hata, A.; Nicholson, E.; Keogan, M.; Fisher, S.; Coleman, E.; Seigler, H. F. Positron emission tomography scanning in malignant melanoma. *Cancer* **2000**, *89*, 1019—1025.

(10) Beatovic, S.; Obradovic, V.; Latkovic, Z.; Jaksic, E. Diagnosis and follow up of primary ocular melanoma by radioimmunoscintigraphy. *J. BUON* **2004**, *9*, 299—302.

(11) Voss, S. D.; Smith, S. V.; DiBartolo, N.; McIntosh, L. J.; Cyr, E. M.; Bonab, A. A.; Dearling, J. L.; Carter, E. A.; Fischman, A. J.; Treves, S. T.; Gillies, S. D.; Sargeson, A. M.; Huston, J. S.; Packard, A. B. Positron emission tomography (PET) imaging of neuroblastoma and melanoma with 64Cu-SarAr immunoconjugates. *Proc. Natl. Acad. Sci. U.S.A.* **2007**, *104*, 17489—17493.

(12) Kato, K.; Kubota, T.; Ikeda, M.; Tadokoro, M.; Abe, S.; Nakano, S.; Nishino, M.; Kobayashi, H.; Ishigaki, T. Low efficacy of 18F-FDG PET for detection of uveal malignant melanoma compared with 123I-IMP SPECT. *J. Nucl. Med.* **2006**, *47*, 404—409.

(13) Cheng, Z.; Xiong, Z.; Subbarayan, M.; Chen, X.; Gambhir, S. S. ^{64}Cu-labeled α-melanocyte-stimulating hormone analog for microPET imaging of melanocortin 1 receptor expression. *Bioconjugate Chem.* **2007**, *18*, 765—772.

(14) Cheng, Z.; Zhang, L.; Graves, E.; Xiong, Z.; Dandekar, M.; Chen, X.; Gambhir, S. S. Small-animal PET of melanocortin 1 receptor expression using a 18F-labeled alpha-melanocyte-stimulating hormone analog. *J. Nucl. Med.* **2007**, *48*, 987—994.

(15) Miao, Y.; Benwell, K.; Quinn, T. P. 99mTc- and 111In-labeled alpha-melanocyte-stimulating hormone peptides as imaging probes for primary and pulmonary metastatic melanoma detection. *J. Nucl. Med.* **2007**, *48*, 73—80.

(16) Ren, G.; Liu, Z.; Miao, Z.; Liu, H.; Subbarayan, M.; Chin, F. T.; Zhang, L.; Gambhir, S. S.; Cheng, Z. PET of malignant melanoma using 18F-labeled metallopeptides. *J. Nucl. Med.* **2009**, *50*, 1865—1872.

(17) Ren, G.; Liu, S.; Liu, H.; Miao, Z.; Cheng, Z. Radiofluorinated rhenium cyclized alpha-MSH analogues for PET imaging of melanocortin receptor 1. *Bioconjugate Chem.* **2010**, *21*, 2355—2360.

(18) Larisch, R.; Schulte, K. W.; Vosberg, H.; Ruzicka, T.; Muller-Gartner, H. W. Differential accumulation of iodine-123-iodobenzamide in melanotic and amelanotic melanoma metastases in vivo. *J. Nucl. Med.* **1998**, *39*, 996—1001.

(19) Chezal, J. M.; Papon, J.; Labarre, P.; Lartigue, C.; Galmier, M. J.; Decombat, C.; Chavignon, O.; Maublant, J.; Teulade, J. C.; Madelmont, J. C.; Moins, N. Evaluation of radiolabeled (hetero)aromatic analogues of N-(2-diethylaminoethyl)-4-iodobenzamide for imaging and targeted radionuclide therapy of melanoma. *J. Med. Chem.* **2008**, *51*, 3133—3144.

(20) Pham, T. Q.; Berghofer, P.; Liu, X.; Greguric, I.; Dikic, B.; Ballantyne, P.; Mattner, F.; Nguyen, V.; Loc'h, C.; Katsifis, A. Preparation and biologic evaluation of a novel radioiodinated benzylpiperazine, 123I-MEL037, for malignant melanoma. *J. Nucl. Med.* **2007**, *48*, 1348—1356.

(21) Eisenhut, M.; Hull, W. E.; Mohammed, A.; Mier, W.; Lay, D.; Just, W.; Gorgas, K.; Lehmann, W. D.; Haberkorn, U. Radioiodinated N-(2-diethylaminoethyl)benzamide derivatives with high melanoma uptake: structure-affinity relationships, metabolic fate, and intracellular localization. *J. Med. Chem.* **2000**, *43*, 3913—3922.

(22) Michelot, J. M.; Moreau, M. F.; Veyre, A. J.; Bonafous, J. F.; Bacin, F. J.; Madelmont, J. C.; Bussiere, F.; Souteyrand, P. A.; Mauclaire, L. P.; Chossat, F. M.; et al. Phase II scintigraphic clinical trial of malignant melanoma and metastases with iodine-123-N-(2-diethylaminoethyl 4-iodobenzamide). *J. Nucl. Med.* **1993**, *34*, 1260—1266.

(23) Ren, G.; Miao, Z.; Liu, H.; Jiang, L.; Limpa-Amara, N.; Mahmood, A.; Gambhir, S. S.; Cheng, Z. Melanin-targeted preclinical PET imaging of melanoma metastasis. *J. Nucl. Med.* **2009**, *50*, 1692—1699.

(24) Garg, S.; Kothari, K.; Thopate, S. R.; Doke, A. K.; Garg, P. K. Design, synthesis, and preliminary in vitro and in vivo evaluation of N-(2-diethylaminoethyl)-4-[18F]fluorobenzamide ([18F]-DAFBA): a novel potential PET probe to image melanoma tumors. *Bioconjugate Chem.* **2009**, *20*, 583—590.

(25) Denoyer, D.; Labarre, P.; Papon, J.; Miot-Noirault, E.; Galmier, M. J.; Madelmont, J. C.; Chezal, J. M.; Moins, N. Development of a high-performance liquid chromatographic method for the determination of a new potent radioiodinated melanoma imaging and therapeutic agent. *J. Chromatogr., B: Anal. Technol. Biomed. Life Sci.* **2008**, *875*, 411—418.

(26) Greguric, I.; Taylor, S. R.; Denoyer, D.; Ballantyne, P.; Berghofer, P.; Roselt, P.; Pham, T. Q.; Mattner, F.; Bourdier, T.; Neels, O. C.; Dorow, D. S.; Loc'h, C.; Hicks, R. J.; Katsifis, A. Discovery of [18F]N-(2-(diethylamino)ethyl)-6-fluoronicotinamide: a melanoma positron emission tomography imaging radiotracer with high tumor to body contrast ratio and rapid renal clearance. *J. Med. Chem.* **2009**, *52*, 5299−5302.

(27) Denoyer, D.; Greguric, I.; Roselt, P.; Neels, O. C.; Aide, N.; Taylor, S. R.; Katsifis, A.; Dorow, D. S.; Hicks, R. J. High-contrast PET of melanoma using (18)F-MEL050, a selective probe for melanin with predominantly renal clearance. *J. Nucl. Med.* **2010**, *51*, 441−447.

(28) Allen-Auerbach, M.; Weber, W. A. Measuring response with FDG-PET: Methodological aspects. *Oncologist* **2009**, *14*, 369−377.

(29) Al Jammaz, I.; Al-Otaibi, B.; Okarvi, S.; Amartey, J. Rapid and efficient synthesis of [F-18]fluoronicotinamides, [F-18]-fluoroisonicotinamides, and [F-18]fluorobenzamides as potential PET radiopharmaceuticals for melanoma imaging. *J. Labelled Compd. Radiopharm.* **2011**, *54*, 312−317.

(30) Cherng, Y. H. Synthesis of substituted pyridines by the reactions of halopyridines with sulfur, oxygen and carbon nucleophiles under focused microwave irradiation. *Tetrahedron* **2002**, *58*, 4931−4935.